Comparative analysis of 2D simulations and isentropic equations for compressible flow in experimental nozzles

San Luis TOLENTINO*,[1,2]

*Corresponding author
[1]National Experimental Polytechnic University "AJS" Vice-Rectorate, Puerto Ordaz (UNEXPO), Bolívar, Venezuela
[2]Group of Mathematical Modeling and Numerical Simulation (GMMNS), National University of Engineering (UNI), Lima, Perú,
sanluist@gmail.com*

DOI: 10.13111/2066-8201.2023.15.3.9

Received: 31 May 2023/ Accepted: 18 July 2023/ Published: September 2023

Abstract: *Experimental studies for supersonic airflow in different supersonic nozzle geometries are recurrent, and the turbulence of the flow can be reproduced with the CFD tool by applying the RANS model and suitable turbulence models. The objective of this investigation is to carry out a comparative analysis of 2D numerical simulation curves for viscous flow with averaged data against equation curves for quasi-one-dimensional isentropic flow, for three experimental supersonic nozzle geometries that are used in the laboratory, for the flow condition without the presence of shock waves in the divergent. For the numerical simulations, three computational domains were discretized with structured grids, the Spalart-Allmaras turbulence model was used, and the Sutherland's law equation was used for the viscosity as a function of temperature. The results of the curve trajectories for Mach number, pressure and temperature obtained with averaged data from the 2D simulations are close to the curves of the analytical and empirical equations for isentropic flow. It is concluded that the numerical error of the total temperature for the planar nozzle with $\alpha = 11.01°$ and NPR = 8.945 reports 0.008%; for the conical nozzle with $\alpha = 15°$ and NPR = 14.925 it reports 1%; and, finally, for the conical nozzle with $\alpha = 4.783°$ and NPR = 7, it reports 0.04%.*

Key Words: *comparative analysis, isentropic flow, Mach number, pressure, temperature, supersonic nozzles, turbulence model, viscous flow*

1. INTRODUCTION

The study of the supersonic flow field in experimental nozzles is recurrent, in order to evaluate the conditions for the development of the flow regime due to the effect of the geometries of the internal walls; where the geometric parameter of the divergent half angle, α, is taken into account in supersonic conical nozzle designs to increase the flow velocity acceleration. Normally, for supersonic conical nozzle designs, the range of $12 \leq \alpha \leq 18°$ is taken into account, for $\alpha < 12°$ they are classified as off-design nozzles [1], [2].

Supersonic nozzle geometries include planar, conical, bell-shaped, parabolic and other types [1].

The distribution of the velocity, pressure, temperature and density gradients are different for each particular geometry, as well as the shapes of the shock wave structures [3], [4].

One of the techniques for imaging shock waves is the Schlieren technique [3]. Pressure data are recorded by arrays of connections distributed at discrete points along the wall, as described in [5], [6], [7], [8]. Both experimental data are important and are taken as reference data to compare the results obtained by numerical simulations with the computational fluid dynamics (CFD) tool [9], [10], [11], generally for 2D and 3D steady-state and transient flow models, as well as to determine the magnitudes of thermodynamic parameters that cannot be measured in experimental tests.

The compressible flow is sensitive to the inlet and outlet pressure variations of the nozzle, therefore, due to the pressure conditions the flow can be over expanded, adapted or under expanded [1], [2]. The supersonic flow exhibits lateral pressure loads on the wall and frictional heating with the wall for a certain thickness in the thermal boundary layer [4], [12], [13], [14], [15]. In the divergent, product of the expansion, the flow decreases the temperature well below the inlet temperature. For an adapted flow, the shock waves do not appear inside the nozzle, however, for an over expanded flow and according to the pressure conditions, the shock appears in the divergent of the nozzle or at its exit, and the shock structure is conditioned to the internal wall curvatures [5], [12], [16], [17].

Experimental studies and CFD numerical simulations with the presence of shock waves in the compressible flow field were reported for different geometries of supersonic nozzles, such as for planar nozzles [5], [7], [8], [18], [19], [20], conical and bell nozzles [6], [13], [16], [21], [22], [23]. Also, other studies have reported results for the 1D flow model using computational codes [24], [25].

For convergent-divergent nozzle geometries, the radius of curvature in the throat section has an effect on the flow development, and relevant related studies for radius of curvatures of the throat section and straight sections of throat length are reported in [22], [26] [27], [28], [29], [30], [31].

The equations for quasi-one-dimensional isentropic compressible flow for conditions without the presence of shock waves at the divergence allow defining the flow patterns of Mach number, pressure, temperature and density, where these curves serve as standard data for the curves obtained by numerical simulations with CFD, as well as to determine the possible deviations that could have certain sections of the curves of the numerical simulations, and the numerical errors that the total temperature presents, being these deviations important for future evaluations of the turbulence model used, the structure of the refined mesh, among other variables.

Likewise, numerical solutions of fluid flow always include three types of errors: modeling errors**,** discretization errors and iteration convergence errors [9], [10], [11], [39]. The motivation of the study focuses on 2D viscous flow and 1D isentropic flow models for three experimental nozzle geometries used in the laboratory. The first is a planar nozzle with $\alpha = 11.01°$ that was studied by Hunter [5] at NASA Langley 16-Foot Transonic Tunnel Complex. The second is a conical nozzle with $\alpha = 15°$ that was studied by Back et al. [32] in research conducted at the Jet Propulsion Laboratory, California Institute of Technology. The third is a conical nozzle with $\alpha = 4.783°$ which was addressed by Carson et al. [33] at the Langley 16-Foot Transonic.

In that sense, in the present investigation, computational simulations of the viscous flow field for Mach number, pressure and steady-state temperature are performed for three computational domains of experimental supersonic nozzle geometries used in the laboratory, in order to carry out a comparative analysis of the numerical simulation curves with the averaged data with respect to the analytical and empirical equation curves for quasi-one-dimensional isentropic flow, where the flow used in the nozzles is air.

Section 2 presents the methodology used. In section 3 the results are discussed. Next, section 4 presents the conclusions.

2. MATERIALS AND METHODS

2.1 Experimental nozzles

The three types of experimental nozzles considered in the investigation are shown in Fig. 1. Fig. 1a illustrates the schematic of a planar nozzle with symmetrical geometry reported by Hunter [5], who performed experimental tests for airflow entering the nozzle at room temperature. Fig. 1b illustrates the schematic of a conical nozzle used by Back et al. [32], in which the flow enters at high temperature and the nozzle wall surface is cooled by the convective heat transfer mechanism through the arrangement of a pipe network system to circulate the water flow.

The ratio of methanol flow rate to air weight was small enough, even for the highest stagnation temperature, so that the combustion products could be treated approximately as air. Also shown in Fig. 1c is a schematic of the geometry of a conical nozzle used by Carson et al. [33] where the airflow enters the nozzle at room temperature, for an axisymmetric variable-geometry nozzle which is applicable for use in the design of the engine for a supersonic cruise aircraft.

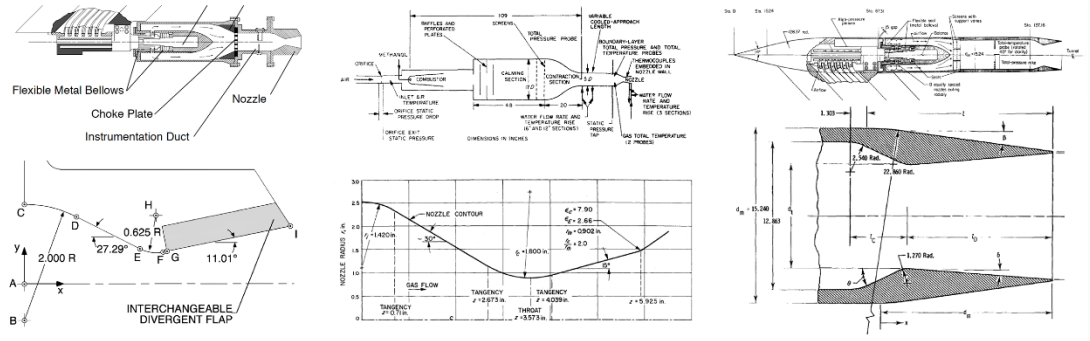

(a) Planar nozzle. Hunter [5]

(b) Conical nozzle. Back et al. [32]

(c) Conical nozzle. Carson et al. [33]

Fig. 1 – Illustration of three supersonic nozzle schemes used in laboratories to obtain experimental pressure data.

2.2 Mathematical fundamentals

For the compressible flow field, the Mach number, M, is the dominant parameter and is classified as: $0.3 \leq M \leq 0.8$ (subsonic flow), $0.8 \leq M \leq 1.2$ (transonic flow), $1.2 \leq M \leq 5$(supersonic flow), $M > 5$ (hypersonic flow) and $M = 1$ (sonic flow) [2]. It should be noted that for values of $M < 0.3$ the flow is considered incompressible.

For the three experimental nozzles that are treated in this work, the flow of air, which is considered as an ideal gas for the compressible flow model, is applied.

For air, the specific heat ratio $k = 1.4$, the specific heat at constant pressure $C_p = 1006.43\ \mathrm{J/(kg \cdot K)}$, the gas constant $R = 287\ \mathrm{J/(kg \cdot K)}$ and the thermal conductivity $k = 0.0242\ \mathrm{W/(m \cdot K)}$ [34].

Analytical and empirical equations for isentropic flow. For supersonic nozzle designs for the quasi-one-dimensional isentropic flow model, the analytical equation (1) [2] is used to determine the Mach number as a function of the area ratio A/A^*, which is expressed as:

$$\frac{A}{A^*} = \frac{1}{M}\left[\left(\frac{2}{k+1}\right) + \left(\frac{k-1}{k+1}\right)M^2\right]^{\left(\frac{k+1}{2k-2}\right)} \quad (1)$$

Equation (1) is very important; it is called the area–Mach number ratio, where k is in the range of $1 < k \leq 1.67$.

In convergent-divergent nozzles for the adapted flow case, the flow passage in the convergent one is accelerated from subsonic to sonic velocity, and in the divergent one from sonic to supersonic. In the throat section the area is defined as critical area A^*, and in this section the flow is throttled down to sonic velocity $M = 1$. At the exit of the nozzle, the exhaust area $A = A_e$, the flow reaches a higher supersonic velocity. Downstream of the nozzle exit, the flow continues to increase in acceleration as a function of the pressure conditions at the nozzle inlet and the pressure conditions of the flow discharge into the ambient atmosphere.

The analytical equation (1) has two solutions, one for supersonic flow and one for subsonic flow; and the said equation is impossible to invert by algebraic procedures, therefore, the calculations of the Mach number are determined by iterative methods. For the solution of the analytical equation (1) for airflow ($k = 1.4$) and Mach number range $1 \leq M \leq 5$, the empirical equation (2) is proposed for supersonic flow, which presents percentage errors lower than 0.0081%, and the empirical equation (3) is proposed for subsonic flow which presents percentage errors lower than 0.0078%. The coefficients and exponents of the empirical equations (2) and (3) were calibrated with Excel 2019 Solver, based on the same methodology reported in [35]. Table 1 presents the coefficients and exponents of equations (2) and (3).

$$M = \left(\frac{A}{A^*}\right)^{n_1}\left[1 + a_1 Ln\left(\frac{A}{A^*}\right)^{n_2}\right]^{n_3} + a_2\left(\frac{A}{A^*}\right)^{n_4}\left[\left(\frac{A}{A^*}\right)^{n_5} - 1\right]^{n_6} \quad (2)$$

$$M = \frac{1}{\left(\frac{A}{A^*}\right)^{n_5}\left[\frac{a_1\left[\left(\frac{A}{A^*}\right)^{n_1} - 1\right]^{n_2}}{\left(\frac{A}{A^*}\right)^{n_3}} + 1\right]^{n_4}} \quad (3)$$

Table 1 – Coefficients and exponents of two empirical equations.

	Supersonic flow: empirical equation (2)					
Coefficient:	a_1	a_2				
	1.297455	3.420083				
Exponent:	n_1	n_2	n_3	n_4	n_5	n_6
	0.02677	0.499652	0.841298	0.082388	0.113979	0.983151
	Subsonic flow: empirical equation (3)					
Coefficient:	a_1					
	0.918866					
Exponent:	n_1	n_2	n_3	n_4	n_5	
	2.007116	0.499844	0.969257	0.840641	0.985639	

The calculation of the pressure ratio P/P_o as a function of Mach number for supersonic and subsonic flow is determined by equation (4) [2], and for the temperature ratio T/T_o by equation (5) [2]:

$$\frac{P}{P_0} = \left[1 + \frac{k-1}{2} M^2\right]^{\left(\frac{k}{1-k}\right)} \tag{4}$$

$$\frac{T}{T_0} = \frac{1}{1 + \frac{k-1}{2} M^2} \tag{5}$$

where P is the static pressure and T is the static temperature, P_o is the total pressure and T_o is the total temperature.

Government equations for viscous flow. The flow field was simulated at a steady state in ANSYS Fluent R16.2 code and the Reynolds-averaged Navier-Stokes equations (RANS) were used.

The governing equations are: the equation of conservation of mass (6), the equation of momentum (7), the equation of energy (8), and the ideal gas equation (9) [34]; in a compact form they are expressed as:

$$\nabla.(\rho u_i) = 0 \tag{6}$$

$$\nabla.\left(\rho u_i u_j\right) = -\nabla p + \nabla.(\bar{\bar{\tau}}) + \nabla.\left(-\rho\overline{u_i' u_j'}\right) \tag{7}$$

$$\nabla.\left(u_i(\rho E + p)\right) = \nabla.\left(k_{eff}\nabla T + \left(\bar{\bar{\tau}}_{eff}.u_i\right)\right) \tag{8}$$

$$p = \rho R T \tag{9}$$

being ρ the density, u the velocity, p the pressure, $\bar{\bar{\tau}}$ the stress tensor, $-\rho\overline{u_i' u_j'}$ the Reynolds stresses, E the total energy, T the temperature, k_{eff} the effective thermal conductivity, $\bar{\bar{\tau}}_{eff}$ is the effective stress tensor and R is the ideal gas constant.

For the modeling of the turbulence of the flow field, the Spalart-Allmaras equation [36] was applied; and for the viscosity as a function of temperature, the Sutherland's law equation [34] was used.

2.3 Structured grids and boundary conditions

Due to the symmetries that the three supersonic nozzles have, the simulation of the flow field in 2D computational domains was considered.

The geometry, the boundary conditions, as well as the structured grids with quadrilateral cells are shown in Fig. 2.

The advantage of using 2D domains is to reduce the computational cost and iteration time of data processing, while for 3D domains the opposite is true. Fig. 2a illustrates the domain for the planar nozzle from Hunter's work [5], where the throat height $h_g = 27.478$ mm and the total length of the nozzle section is $L_{total} = 115.57$ mm; a section of the atmosphere with a length of 254 mm is not shown in the domain.

For the conical nozzle from the work of Back et al. [32], the domain is shown in Fig. 2b, with a throat diameter $D_g = 45.816$ mm and a total length $L_{total} = 150.495$ mm. Likewise, Fig. 2c shows the domain for the conical nozzle from the work of Carson et al. [33], with throat diameter $D_g = 90.2208$ mm and total length $L_{total} = 168.552$ mm.

It should be noted that the detailed dimensions for each supersonic nozzle geometry shown in Fig. 2 are reported individually by each author mentioned.

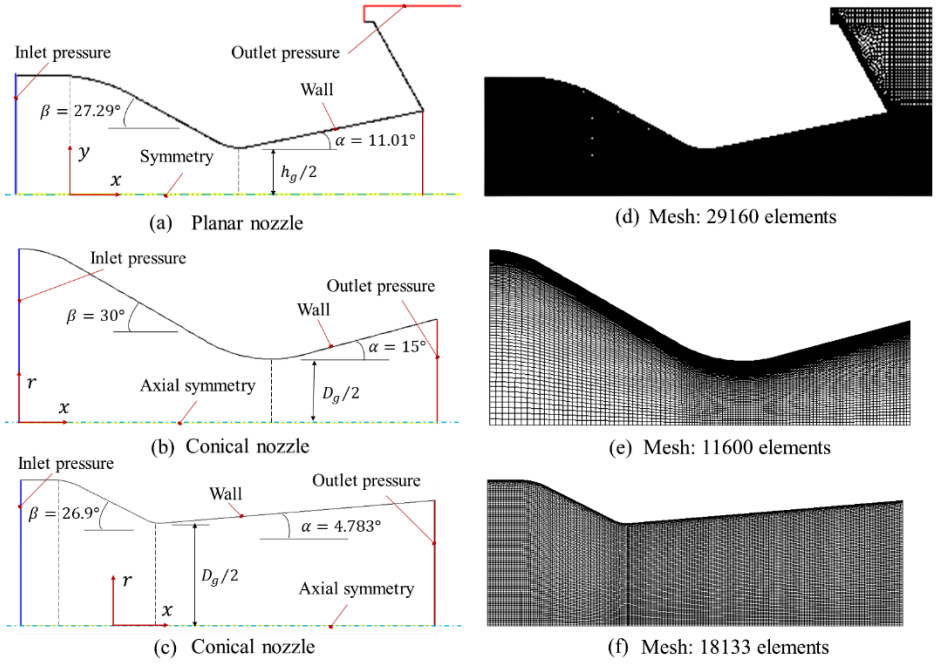

Fig. 2 – Geometry, boundary conditions and structured grids for the three experimental nozzles: (a) and (d) Planar nozzle with $\alpha = 11.01°$ [5], (b) and (e) Conical nozzle with $\alpha = 15°$ [32] and (c) and (f) Conical nozzle with $\alpha = 4.783°$ [33]

Table 2 presents the pressure and temperature data for the application of the boundary conditions for the three computational domains shown in Fig. 1a, Fig. 1b and Fig. 1c.

It should be noted that for the computational domains of the two conical nozzles in axial symmetry the flow velocity in the radial direction is zero, and in the vertical direction it is zero for the planar nozzle.

On the walls of the three nozzles the flow velocity is zero due to the no-slip condition. For the planar nozzle wall with $\alpha = 11.01°$ (Fig. 2a) is considered to be adiabatic, $\dot{Q} = 0$, as well as for the conical nozzle with $\alpha = 4.783°$ (Fig. 2c); whereas, for the conical nozzle with $\alpha = 15°$ (Fig. 2b) the wall is not adiabatic, $\dot{Q} \neq 0$. Where, $\dot{Q}$ is the heat flux.

The effect of gravity is not taken into account for all three computational domains, since the flow behavior is modelled in 2D.

Table 2 – Boundary conditions for the three experimental nozzle geometries shown in Fig. 2.

Nozzle	Inlet		Outlet		Wall	NPR
	P_o [kPa]	T_o [K]	P [kPa]	T [K]		
Planar [5]	915.874	294.444	102.3895	294.444	$\dot{Q} = 0$	8.945
Conical [32]	1038.35	824.4445	69.56948	412.2222	412.222 K	14.925
Conical [33]	700	300	100	300	$\dot{Q} = 0$	7

For numerical convergence, a sensitivity study of the mesh with quadrilateral cells was carried out on the ANSYS-Meshing platform, where the domains were discretized by the finite volume method (FVM); for which three turbulence models were used: S-A of Spalart-Allmaras [36], SST $k - \omega$ of Menter [37] and $k - \omega$ of Wilcox [38]. Each domain was refined three times and the optimal mesh was obtained for the third structured grids and are shown in

Fig. 2d, Fig. 2e and 2f. For the optimal meshes, the S-A turbulence model [36] presented better results with respect to the SST $k-\omega$ [37] and $k-\omega$ [38] turbulence models, where these three turbulence models were compared with experimental data from pressure evaluated on the walls; As well as for variations of y^+ in the shear stress value for the flow region adjacent to the nozzle wall.

The pressure for the planar nozzle with $\alpha = 11.01°$ and NPR = 8.945 is shown in Fig. 3a, and for y^+ it is shown in Fig. 3d which shows $y^+ < 100$; the throat is located at position $x/x_t = 1$ and the nozzle outlet at position $x/x_t = 2$, where $x_t = 57.785$ mm.

The pressure for the conical nozzle with $\alpha = 15°$ and NPR = 14.925 is shown in Fig. 3b, and for y^+ it is shown in Fig. 3e to have $y^+ < 40$; the throat is located at $x/L_{total} = 0.6025$ and the nozzle outlet at $x/L_{total} = 1$, with $L_{total} = 150.495$ mm.

Likewise, the pressure for the conical nozzle with $\alpha = 4.783$ and NPR = 7 is shown in Fig. 3c, and for y^+ it is shown in Fig. 3f where $y^+ < 250$; the throat is located at $x/D_m = 0.203$ and the nozzle outlet at $x/D_m = 1$, where $D_m = 152.4$ mm.

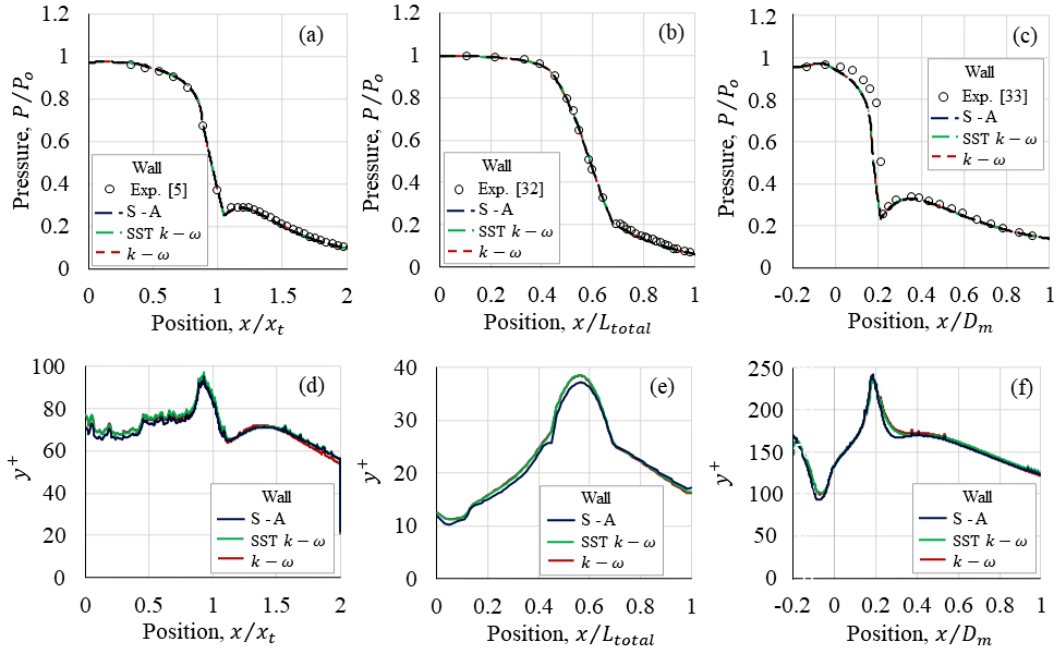

Fig. 3 – Experimental data curves of pressure and y^+ at the walls of the three experimental nozzles for three turbulence models. (a) and (d) Planar nozzle, for $\alpha = 11.01°$ and NPR = 8.945. (b) and (e) Conical nozzle, for $\alpha = 15°$ and NPR = 14.925. (c) and (f) Conical nozzle, for $\alpha = 4.783$ and NPR = 7

2.4 Computational solution method

In ANSYS-Fluent R16.2 the following considerations were taken into account:

In Solver: Type: density -based; Velocity formulation: absolute; Time: steady; 2D space: planar and axisymmetric. In models: Energy and Spalart-Allmaras turbulence model. In Materials: air, and Sutherland's law was used for flow viscosity as a function of temperature. In Solution methods: Formulation: implicit; Flux type: Roe-FDS; Spatial discretization: Gradient: Least Squares Cell Based; Flow: Second Order Upwind; and, Modified turbulent viscosity: Second Order Upwind. For the mass balance control, the mass flow rate was taken into account, for an error in the range of $1x10^{-5}$ to $1x10^{-6}$. The hybrid initialization method was

applied. Run calculation: from 13350 to 35000 iterations were performed to obtain the final results of the Mach number, pressure and temperature flow field.

A computer with the following characteristics was used for data processing: OptiPlex 7010 model, i5 3470 (Dell CPU), two 3.2 GHz processors, and 8 GB of RAM memory.

2.5 Procedure to obtain trajectories of curves

In the case of the trajectories of the curves of the isentropic flow model for the three experimental nozzle geometries studied, we proceeded as follows: to obtain the Mach number curves, the cross-sectional areas of the nozzles in the convergent and divergent sections were taken as reference, and with equation (1) the Mach number per iteration was determined.

To obtain the static pressure and static temperature curves, the previously calculated Mach number was substituted into equation (4) and equation (5).

Then, to obtain the approximate solution curves obtained with the empirical equations, equation (4) was used for the subsonic flow and equation (3) for the supersonic flow. And to obtain the static pressure and static temperature curves, the empirical equations (2) and (3) were substituted into the analytical equations (4) and (5).

For the case of the viscous flow model that was simulated in 2D in ANSYS-Fluent R16.2, the curves (2D avg.) of the Mach number, static pressure and static temperature were constructed with 2D average values.

The 2D average values were obtained by discretizing the flow into several cross sections in the radial direction for the conical nozzles, and transverse for the planar nozzle, from the inlet to the outlet of the nozzle, then, for each cross section that is normal to the flow direction the average was calculated by the numerical integration method with the option: area-weighted average in ANSYS-Fluent.

Subsequently, for the analysis, the curves of the simulations (2D avg.) and the curves of the isentropic flow (1D), as well as the experimental pressure data, were grouped together. It should be noted that the static pressure and Mach number curves for the non-averaged data are included in the graphs; where, all curves were edited in an Excel 2019 spreadsheet.

3. RESULTS AND DISCUSSIONS

The Mach number, static pressure and static temperature flow fields are illustrated in Fig. 4a, 4b and 4c, the red region is of higher magnitude and the blue region is of lower magnitude; and the curve trajectories and experimental pressure data are shown in Fig. 5, 6 and 7. For the conical nozzle and NPR = 7 (Fig. 4c), the flow presents internal shock with greater intensity in the divergent, and it is observed how the oblique and reflected wave is distributed. In the central region of the flow, where the waves intersect, there is a strong fluctuation that causes the flow to decelerate. For the flat nozzle with y NPR = 8.945 (Fig. 4a), the fluctuation is smooth. Whereas, for the conical nozzle with y NPR = 14.925 (Fig. 4b), the flow does not fluctuate.

For the planar nozzle with $\alpha = 11.01°$ and NPR = 8.945 (Fig. 4a) the fluctuation is smooth, and for the conical nozzle with $\alpha = 15°$ and NPR = 14.925 (Fig. 4b) the flow does not fluctuate.

With respect to the flow patterns of curved paths and experimental data of pressure on the walls of the planar nozzle with $\alpha = 11.01°$ and NPR = 8.945 shown in Fig. 5a, the throat is located at the position $x/x_t = 1$ and the nozzle outlet at position $x/x_t = 2$.

For the conical nozzle with $\alpha = 15°$ and NPR = 14.925 shown in Fig. 6a, the throat is located at $x/L_{total} = 0.6025$ and the nozzle outlet at $x/L_{total} = 1$, thus as, for the conical

nozzle Fig. 7a shows a nozzle with $\alpha = 4.783°$ and NPR = 7, the throat is located at $x/D_m = 0.203$ and the nozzle outlet at $x/D_m = 1$.

With respect to the static pressure P/P_o, in Fig. 5a, 6a and 7a the trajectories of the curves of the 2D numerical simulations at the wall are close and superimposed to the experimental pressure data, whereas, the curves of the simulations in the symmetry have stretches away from the experimental data.

The trajectories of the curves obtained with the analytical equations and the empirical equations also show that certain sections of the curves are superimposed on the experimental data. The one with the largest pressure fluctuation in symmetry within the estimated positions from $x/D_m = 0.65$ to $x/D_m = 0.72$, is for the conical nozzle with $\alpha = 4.783°$ and NPR = 7 shown in Fig. 7a.

While, with respect to the curves of the 2D numerical simulations obtained in the symmetry, the Mach number for the planar nozzle, illustrated in Fig. 5b, shows a fluctuation close to the estimated position $x/x_t = 1.5$; for the conical nozzle shown in Fig. 6b it shows no fluctuation, so the flow is continuously accelerated up to the nozzle exit.

While for the conical nozzle shown in Fig. 7b, the Mach number shows a deceleration of the flow within the estimated positions from $x/D_m = 0.65$ to $x/D_m = 0.72$, which is evident in the flow field for the Mach number distribution shown in Fig. 4c.

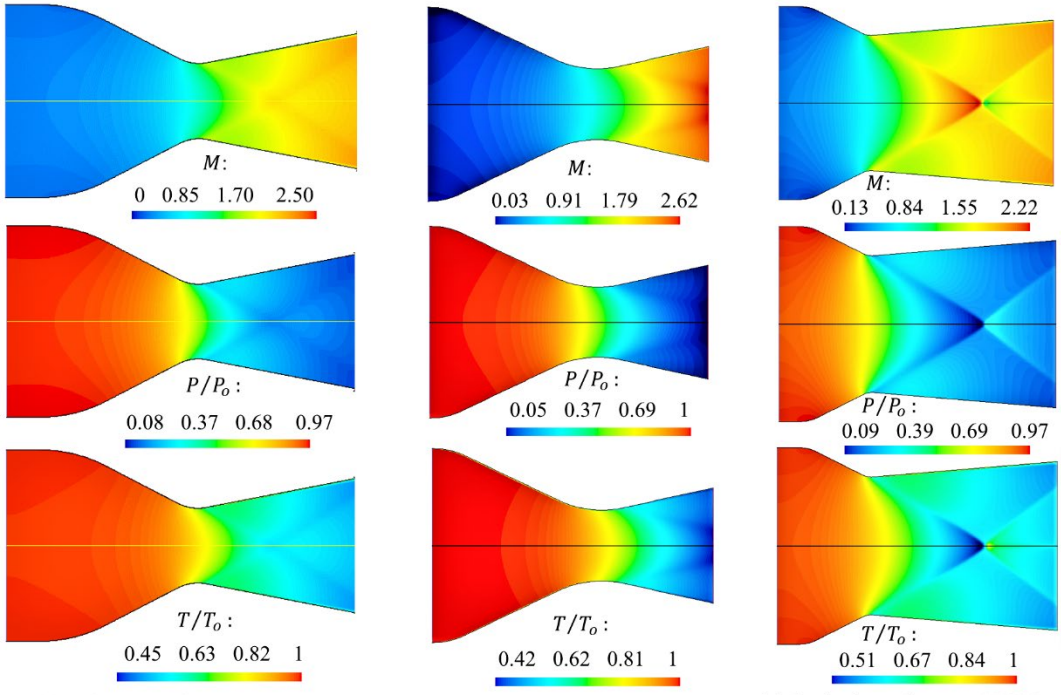

(a) Planar nozzle. $\alpha = 11.01°$, NPR = 8.945

(b) Conical nozzle. $\alpha = 15°$, NPR = 14.925

(c) Conical nozzle. $\alpha = 4.783°$, NPR = 7

Fig. 4 – Flow field: (a) Mach number, (b) static pressure and (c) static temperature for three types of experimental supersonic nozzles. The red region is of higher magnitude and the blue region is of lower magnitude

The trajectories of the numerical curves (2D avg.) obtained with the average data of static pressure (Fig. 5c, 6c and 7c), Mach number (Fig. 5d, 6d and 7d) and static temperature (5e, 6e and 7e) show how they are distributed over the curves of the analytical and empirical equations for the isentropic flow.

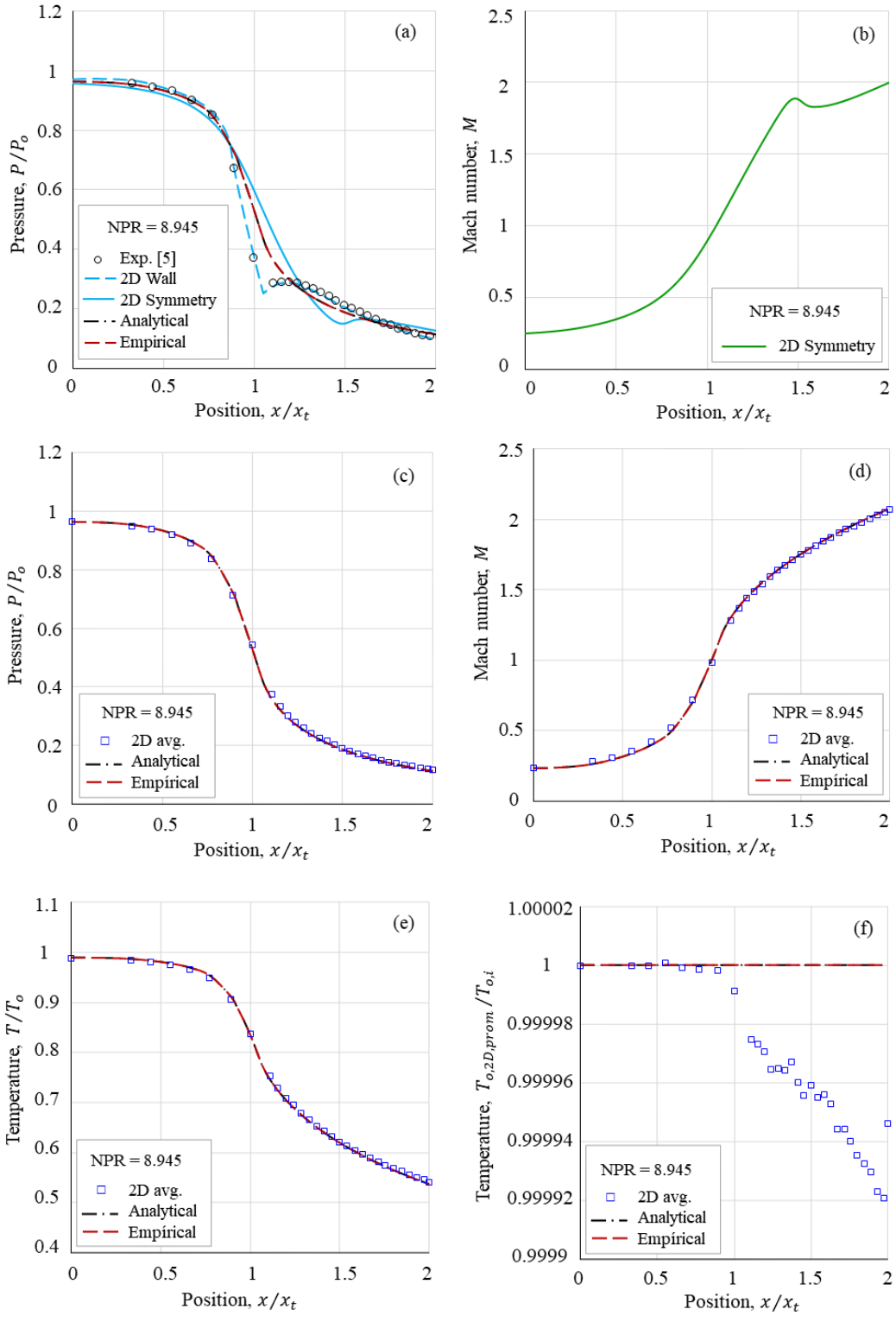

Fig. 5 – Trajectories of curves of Mach number, static pressure, static temperature and total temperature for the geometry of a planar nozzle [5], $\alpha = 11{,}01°$ and NPR = 8.945. Throat position $x/x_t = 1$

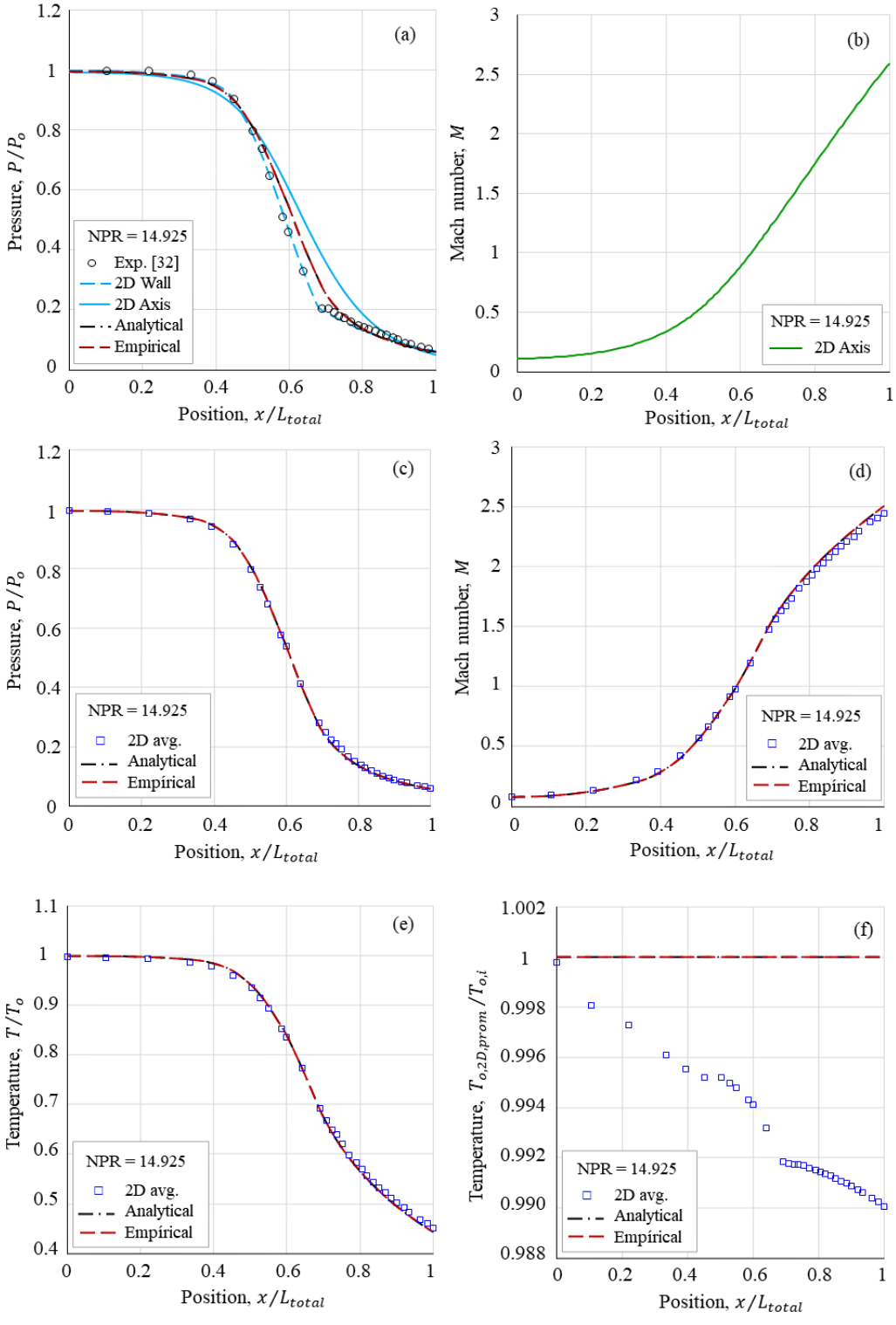

Fig. 6 – Trajectories of curves of Mach number, static pressure, static temperature and total temperature for the geometry of a conical nozzle [32], $\alpha = 15°$ and NPR = 14.925. Throat position $x/L_{total} = 0{,}6025$

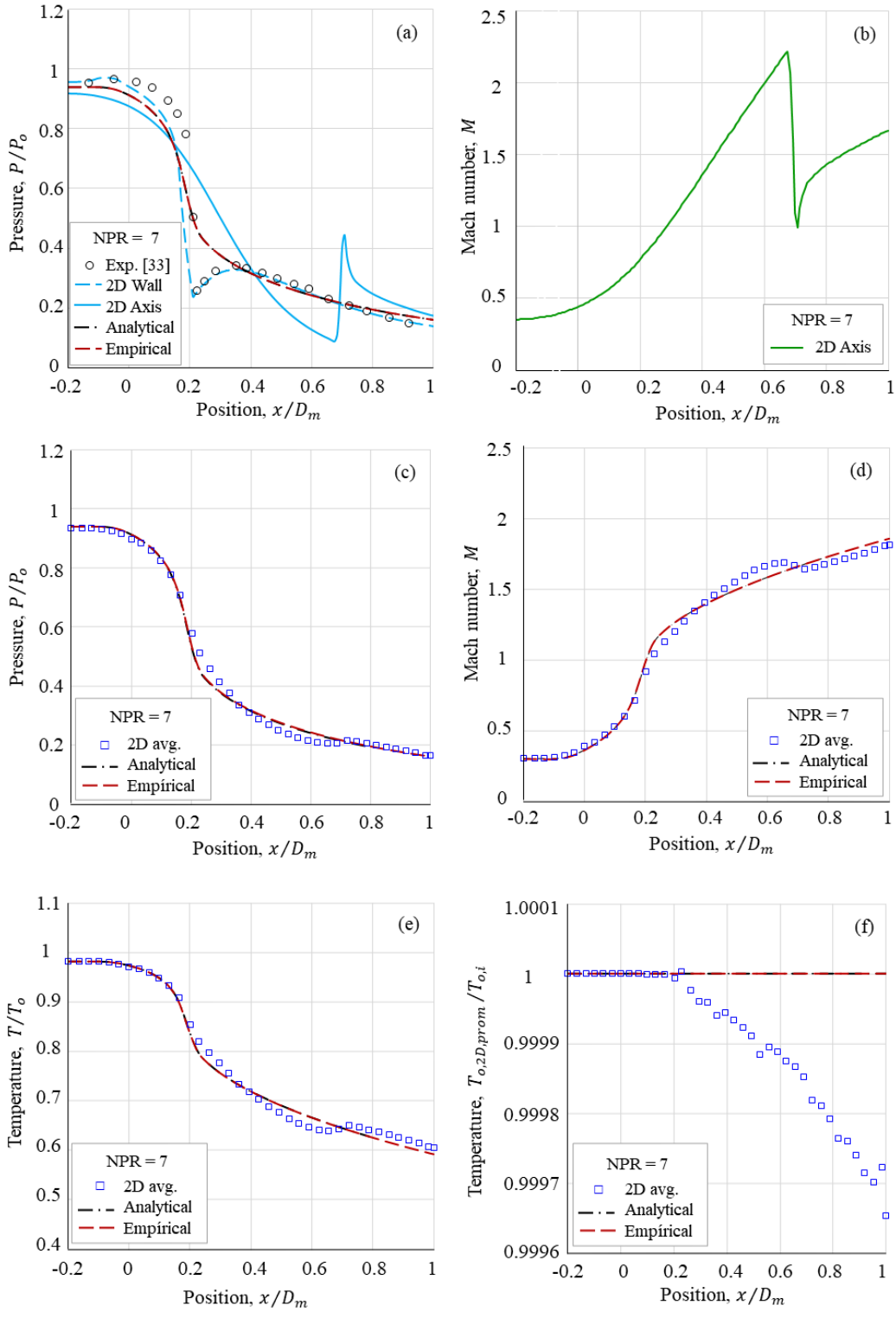

Fig. 7 – Trajectories of curves of Mach number, static pressure, static temperature and total temperature for the geometry of a conical nozzle [33], $\alpha = 4.783°$ and NPR = 7. Throat position $x/D_m = 0.203$

The simulation data (2D avg.) with the best fit to the analytical and empirical equation curves are for the planar nozzle with $\alpha = 11.01°$ and NPR = 8.945 (Fig. 5) which was simulated with adiabatic walls, where the flow at the nozzle outlet for Mach number gives an percentage error of 0.666%, for static pressure an error of 0.534% and for static temperature an error of 0.797%. While, for the conical nozzle with $\alpha = 15°$ and NPR = 14.925 (Fig. 6) with non-adiabatic wall, the flow at the nozzle outlet for the Mach number gives the percentage error of 2.323%, for the static pressure an error of 4.567% and for the static temperature an error of 0.328%. For the conical nozzle with $\alpha = 4.783°$ and NPR = 7 (Fig. 7), the numerical results of static pressure (Fig. 7c), Mach number (Fig. 7d) and static temperature (Fig. 7e) fluctuate around from the curves of the analytical and empirical equations in the estimated range of $0{,}4 < x/D_m < 0{,}75$; where the flow at the nozzle outlet for the Mach number gives a percentage error of 2.265%, for the static pressure an error of 1.324% and for the static temperature an error of 1.995%. Based on these results in the mentioned range, this fluctuation could be affected by the conditions of the internal shock for $\alpha = 4.783°$, which lead to variations in the magnitudes of the thermodynamic parameters of the flow in the central region and adjacent to the wall of the nozzle, as well as by the non-inclusion of the flow outside the nozzle. Therefore, it is considered that a more exhaustive study should be carried out and take into account all the variables and parameters involved in the internal flow and external flow in order to reduce the error, since in operating conditions of the experimental data collections a flow out of the nozzle is present according to the experiments of Carson et al. [33].

The ratio of the total temperature taking into account the total temperature $T_{o,2D\ avg}$ from the numerical results (2D avg.) over the total temperature $T_{o,i}$ from the analytical or empirical equation for isentropic flow should be equal or very close to unity $T_{o,2D\ avg}/T_{0,i} \cong 1$. This is because in certain regions of the flow field, the computational simulations present numerical errors due to the density of the mesh, the numerical precision in the number of exact decimal digits, the turbulence model used, the thermal energy loss of the flow through the walls, among other variables. In addition, numerical solutions of fluid flow and heat transfer problems always include three types of errors, which are listed below: a) modeling errors, b) discretization errors, and c) iteration convergence errors. The ratio of the total temperature $T_{o,2D\ avg}/T_{0,i}$ shown in Fig. 5f, 6f and 7f, evidences the increase of the numerical errors as the flow moves towards the nozzle outlet. For the case of the planar nozzle (Fig. 5f), for the average total temperature (2D avg.) along the nozzle the percentage error is less than 0.008%, where $0.99992 \leq T_{o,2D\ avg}/T_{oi} \leq 1$. For the case of the conical nozzle (Fig. 7f) the error is less than 0.04%, where $0.9996 \leq T_{o,2D\ avg}/T_{oi} \leq 1$. Where both nozzles that were simulated with adiabatic walls, therefore the percentage errors are very small.

While for the case of the conical nozzle (Fig. 6f) where the flow was simulated for non-adiabatic walls, the error is less than 1% for the total temperature ratio, where $0.99 \leq T_{o,2D\ avg}/T_{oi} \leq 1$. This 1% error is larger with respect to the planar nozzle with $\alpha = 11.01°$ which has 0.008% and the conical nozzle with $\alpha = 4.783$ which has 0.04%. The constant temperature set at the wall affects the flow development in the thermal boundary layer region as well as the temperature rise at the divergent wall due to flow friction. Therefore, it is considered that another study should be addressed by evaluating along the nozzle wall for a temperature gradient and taking into account the amount of heat extracted by convection, as indicated in the experiment of Back et al. [32]. However, according to the results obtained for the Mach number, static pressure and static temperature for the numerical simulations with averaged data (2D avg.) are satisfactory as they follow the trajectory of the curves of the analytical and empirical equations used for the quasi-one-dimensional isentropic flow model.

4. CONCLUSIONS

The simulations of the viscous flow field for the three experimental nozzles present different wall pressure patterns, which reproduce the decays and increases of the experimental pressure data.

The trajectories of the curves (2D avg.) of the Mach number, static pressure, static temperature and total temperature parameters approximate the solutions of the analytical and empirical equations used for quasi-one-dimensional isentropic flow.

The flow at the nozzle outlet, for the planar nozzle with $\alpha = 11{,}01°$ and NPR = 8.945, the Mach number has an error of 0.666%, and the total temperature has an error of 0.008%.

For the conical nozzle with $\alpha = 15°$ and NPR = 14.925, the Mach number has an error of 2.323%, and the total temperature has an error of 1%.

Finally, for the conical nozzle with $\alpha = 4{,}783°$ and NPR = 7, the Mach number gives an error of 2.265%, and the total temperature an error of 0.04%.

REFERENCES

[1] G. P. Sutton and O. Biblarz, *Rocket propulsion elements,* New York, John Wiley and Sons, 2016.

[2] J. D. Anderson, *Fundamentals of aerodynamics*, New York, McGraw-Hill Education, 2017.

[3] P. Krehl and S. Engemann, August Toepler - the first who visualized shock waves, *Shock Waves*, vol. **5**, no. 1, pp. 1–18, 1995. https://doi.org/10.1007/BF02425031

[4] H. Schlichting and k. Gersten, *Boundary-layer theory*, Berlin Heidelberg, Germany, Springer Verlag, 9th ed., 2017.

[5] C. A. Hunter, Experimental, theoretical, and computational investigation of separated nozzle flows, *34th AIAA/ASME/SAE/ASEE Joint Propulsion Conference & exhibit*, Cleveland, OH, July 1998, https://doi.org/10.2514/6.1998-3107

[6] R. Stark and G. Hagemann, Current status of numerical flow prediction for separated nozzle flows, *2 European Conference For Aerospace Sciences (Eucass),* 2007.

[7] S. B. Verma, C. Manisankar, Origin of flow asymmetry in planar nozzles with separation, *Shock Waves,* vol. **24**, pp. 191-209, 2014, https://doi.org/10.1007/s00193-013-0492-1

[8] S. Živković, M Milinović and N. Adamec, Experimental and numerical research of a supersonic planar thrust vectoring nozzle via mechanical tabs, *FME Transactions*, vol. **42**, no. 3, pp. 205-211, 2014, https://doi.org/10.5937/fmet1403205Z

[9] J. D. Anderson, *Computational fluid dynamics: The basics with applications*, McGraw-Hill Series in Mechanical Engineering, 1995.

[10] J. Blazek, *Computational fluid dynamics: Principles and applications*, Oxford, United Kingdom: Butterworth-Heinemann, 2015.

[11] J. H. Ferziger, M. Perić and R. L. Street, *Computational Methods for Fluid Dynamics*, Springer, 2020.

[12] M. Frey, G. Hagemann, Flow separation and side loads in rocket nozzles, *AIAA 99-2815, 35th Joint Propulsion Conference and Exhibit,* 1999.

[13] J. Östlund and B. Muhammed, Supersonic flow separation with application to rocket engine nozzles, *ASME, Applied Mechanics Reviews*, vol. **58**, no. 3, pp. 143–177, 2005, doi: https://doi.org/10.1115/1.1894402

[14] A. Aghababaie and R. Theunissen, "Modeling free shock separation induced side loads in overexpanded rocket nozzles," *AIAA Journal* **53**, 2015, https://doi.org/10.2514/1.J053014

[15] C. Génin and R. Stark, Hot Flow Testing of Dual Bell Nozzles, In *49th AIAA Aerospace Sciences Meeting Including the New Horizons Forum and Aerospace Exposition,* 2011, pp. 1-8, https://doi.org/10.2514/6.2011-387

[16] V. Zmijanović, B. Rašuo, A. Chpoun, Flow separation modes and side phenomena in an overexpanded nozzle, *FME Transactions*, vol. **40**, no. 3, pp. 111-118, 2012.

[17] A. Shams, S. Girard and P. Comte, Numerical simulation of shock-induced separated flows in over expanded rocket nozzles, *Progress in Flight Physics*, vol. **3**, pp. 169-190, 2012. https://doi.org/10.1051/eucass/201203169

[18] R. Arora, R. Vaidyanathan, Experimental investigation of flow through planar double divergent nozzles, *Acta Astronautica,* vol. **112**, pp. 200-216, 2015.

[19] S. L. Tolentino, Evaluation of turbulence models for the air flow in a planar nozzle, *Ingenius,* no. 22, pp. 25–37, 2019. https://doi.org/10.17163/ings.n22.2019.03
[20] Y. Li, Ch. He, J. Li, L. Miao, R. Gao, J. Liang, Experimental investigation of flow separation in a planar convergent-divergent nozzle, *Journal of Physics: Conference Series, 1300, 012088*, 2019, https://doi.org/10.1088/1742-6596/1300/1/012088
[21] R. Jia, Z. Jiang, W. Zhang, Numerical analysis of flow separation and side loads of a conical nozzle during staging, *J. Aerospace Engineering*, vol. **230**, no. 5, pp. 845-855, 2016. https://doi.org/10.1177/0954410015599798
[22] S. L. Tolentino and J. Mírez, Throat length effect on the flow patterns in off-design conical nozzles, *FME Transactions*, vol. **50**, no. 2, pp. 271-282, 2022. https://doi.org/10.5937/fme2201271T
[23] C. Jéger and Á. Veress, Novell Application of CFD for Rocket Engine Nozzle Optimization, *Periodica Polytechnica Transportation Engineering*, vol. **47**, no. 2, pp. 131-135, 2019. https://doi.org/10.3311/PPtr.11490
[24] F. Gaitan, Finding flows of a Navier–Stokes fluid through quantum computing, *Npj Quantum Information*, vol. **6**, pp. 1-6, 2020. https://doi.org/10.1038/s41534-020-00291-0
[25] L. Gascón, J. M. Corberán and J. A. García-Manrique, Numerical schemes for quasi-1D steady nozzle flows, *Applied Mathematics and Computation*, vol. **400**, pp. 1-14, 2021. https://doi.org/10.1016/j.amc.2021.126072
[26] A. Sauer, General characteristics of the flow through nozzles at near critical speeds, *NACA TM-1147,* 1947.
[27] R. F. Cuffel, L. H. Back and P. F. Massier, Transonic flowfield in a supersonic nozzle with small throat radius of curvature, *AIAA Journal*, vol. **7**, no. 7, pp. 1364–1366, 1969. https://doi.org/10.2514/3.5349
[28] R. Kliegel and J. N. Levine, Transonic flow in small throat radius of curvature nozzles, *AAIA Journal*, vol. **7**, no. 7, pp. 1375-1378, 1969.
[29] S. L. Tolentino and J. Mírez, Numerical analysis of over-expanded flow in the experimental ULA-2 conical nozzle out of design, *Lámpsakos*, no **24**, pp. 33-47, 2020, (in Spanish). https://doi.org/10.21501/214540863707
[30] C.E. Rogers, The solid rocket motor-Part 4. Departures from ideal performance for conical nozzles and bell nozzles, straight-cut throats and rounded throats, *Tech series, High Power Rocketry*.
[31] S. L. Tolentino and O. González, Numerical analysis of the over-expanded flow in the experimental conical nozzle ULA-1B out of design, *Lámpsakos*, no **24**, pp. 33-47, 2021, (in Spanish). https://doi.org/10.21501/214540863707
[32] L. H. Back, P. F. Massier and H. L. Gier, Convective heat transfer in a convergent-divergent nozzle, *Technical Report No. 32-475*, pp. 1-55, 1965.
[33] G. T. Carson, E. E. Lee, Experimental and analytical investigation of axisymmetric supersonic cruise nozzle geometry at Mach numbers from 0,60 to 1,30, *NASA Technical paper 1953,* December, pp. 1-90, 1981.
[34] * * * ANSYS. *Ansys Fluent Theory guide* v. **14**, November 2011, Available at https://kargosha.com/file/attach/201705/2812.pdf
[35] S. L. Tolentino, Empirical equation of the Mach number as a function of the stagnation pressure ratio for a quasi-one-dimensional compressible flow, *FME Transactions*, vol. **51**, no. 2, pp. 149-160, 2023. https://doi.org/10.5937/fme2302149T
[36] P. R. Spalart and S. R. Allmaras, A one-equation turbulence model for aerodynamic flows, *30th Aerospace Sciences Meeting and Exhibit, 06 January 1992 – 09*, Reno, NV, U.S.A, 1992, pp. 1-22. https://doi.org/10.2514/6.1992-439
[37] F. R. Menter, Two equation eddy-viscosity turbulence models for engineering applications, *AIAA Journal*, vol. **32**, no. 8, pp. 1598–1605, 1994. https://doi.org/10.2514/3.12149
[38] D. C. Wilcox, Reassessment of the scale-determining equation for advanced turbulence models, *AIAA Journal*, vol. **26**, no. 11, pp. 1299–1310, 1988. https://doi.org/10.2514/3.10041
[39] Z. Lilek and M. Perić, A fourth-order finite volume method with colocated variable arrangement, *Computers and Fluid,* vol. **24**, no. 3, pp. 239-252, 1995.